

PENALIZED LEAST SQUARES METHODS FOR SOLVING THE EEG INVERSE PROBLEM

Mayrim Vega-Hernández, Eduardo Martínez-Montes,

José M. Sánchez-Bornot, Agustín Lage-Castellanos

and Pedro A. Valdés-Sosa

Cuban Neuroscience Center

Abstract: Most of the known solutions (linear and nonlinear) of the ill-posed EEG Inverse Problem can be interpreted as the estimated coefficients in a penalized regression framework. In this work we present a general formulation of this problem as a Multiple Penalized Least Squares model, which encompasses many of the previously known methods as particular cases (e.g., Minimum Norm, LORETA). New types of inverse solutions arise since recent advances in the field of penalized regression have made it possible to deal with non-convex penalty functions, which provide sparse solutions (Fan and Li (2001)). Moreover, a generalization of this approach allows the use of any combination of penalties based on l_1 or l_2 -norms, leading to solutions with combined properties such as smoothness and sparsity. Synthetic data is used to explore the benefits of non-convex penalty functions (e.g., LASSO, SCAD and LASSO Fusion) and mixtures (e.g., Elastic Net and LASSO Fused) by comparing them with known solutions in terms of localization error, blurring and visibility. Real data is used to show that a mixture model (Elastic Net) allows for tuning the spatial resolution of the solution to range from very concentrated to very blurred sources.

Key words and phrases: EEG, inverse problem, least squares, penalized regression.

1. Introduction

The identification of the neural current sources inside the brain generating the voltage field measured over an array of sensors distributed on the scalp surface is known as the Inverse Problem (IP) of the Electroencephalography (EEG). The mathematical relation between these voltages (\mathbf{v}) and the Primary Current Density (PCD, \mathbf{j}) is given by

$$\mathbf{v}_{(Ne \times 1)} = \mathbf{K}_{(Ne \times 3Ng)} \mathbf{j}_{(3Ng \times 1)} + \boldsymbol{\varepsilon}_{(Ne \times 1)}, \quad (1.1)$$

where the noisy nature of the EEG recordings is explicitly taken into account through the vector of errors ($\boldsymbol{\varepsilon}$). The number of sensors or electrodes is Ne and the number of sources Ng correspond to the number of grid points of the

discretization of the source space inside the brain. The $3Ng$ elements of the column vector $\mathbf{j} = [j_{1x}, j_{1y}, j_{1z}, \dots, j_{Ngx}, j_{Ngy}, j_{Ngz}]^T$ correspond to the three components of the PCD vector field for each point in the grid. The matrix \mathbf{K} is known as the electric lead field, and summarizes the geometric and electric properties of the conducting media (brain, skull and scalp).

Usually $Ng \gg Ne$ and so the IP of the EEG is an ill-posed problem in the sense of Hadamard, due to the non-uniqueness of the solution (Hadamard (1923)). The non-uniqueness naturally arises from the underdetermination of the system, but the Lead Field matrix \mathbf{K} is usually ill-conditioned as well, which means that small changes in the data can lead to totally different PCD configurations as inverse solutions. To overcome the non-uniqueness one is forced to use additional data-independent information, also known as prior information, which can reflect anatomical, physical and/or mathematical properties of the current sources inside the head.

Current methods for solving the IP of EEG are based on different kind of prior information used, and can be divided into two groups: **dipole solutions** which assume that the PCD is a set of current dipoles (Scherg and von Cramon (1986) and Scholz and Schwierz (1994)), and **distributed inverse solutions** which assume that the current density is distributed widely within the brain (Hämäläinen and Ilmoniemi (1994) and Pascual-Marqui, Michel and Lehmann (1994)). The former are appropriate in cases where small areas are expected to be activated but suffer from a subjective bias since the number of dipoles is fixed by the researcher. On the other hand, distributed inverse solutions are more plausible in cognitive states involving wide areas in the brain as well as in spontaneous and pathological activities. The modelling in this group has dramatically evolved from simple 2D approaches (Hämäläinen and Ilmoniemi (1994)) to more sophisticated 3D implementations (Fuchs, Wagner, Wischman and Dossel (1995), Pascual-Marqui, Michel and Lehmann (1994), Valdés-Sosa, Marti, Garcia and Casanova (2000) and Trujillo-Barreto, Aubert-Vázquez and Valdés-Sosa (2004)).

Several distributed inverse solutions are found through the use of Tikhonov regularization. Some of them are presented in Table 1 of the supplemental material (online) with the abbreviation to be used for referring to them. They are computed as the PCD which minimizes a particular functional of the form

$$\hat{\mathbf{j}} = \arg \min \left\{ \|\mathbf{v} - \mathbf{K}\mathbf{j}\|_2^2 + \lambda^2 \|\mathbf{H}\mathbf{j}\|_2^2 \right\} \quad (1.2)$$

for a given regularization parameter λ . This parameter represents the relative weight between the data fitting error and prior terms, and can be calculated by cross validation (Craven and Wahba (1979)) or by the L-curve method (Hansen (1992)). Herein the symbol $\|\cdot\|_p$ denotes the lp -norm. Different prior assumptions

about the solution are given by the choice of \mathbf{H} (see Pascual-Marqui (1999) for a review). Two important and popular cases are known as Minimum Norm (MN) (Hämäläinen and Ilmoniemi (1994)) and Low Resolution Electromagnetic Tomography (LORETA) (Pascual-Marqui, Michel and Lehmann (1994)), which choose \mathbf{H} as the identity matrix and the discrete Laplacian operator, respectively (see the definition in Table 2 of the online supplemental material).

The functional (1.2) can also be interpreted as a penalized least squares regression, in which the penalty term (prior) is a quadratic function of coefficients to estimate (\mathbf{j}). This is known in the linear regression field as ridge regression with different operators \mathbf{H} (Hoerl and Kennard (2000)), that offer smooth solutions. However, recent advances in penalized least squares regression have brought attention to the use of non-convex penalty functions, which can produce sparser or more concentrated solutions (Fan and Li (2001)). Definitions and properties of non-convex functions are recalled in the Section 1 of the online supplemental material. These are non-quadratic functions of the coefficients to estimate, usually based on their l_1 -norm. Moreover, it has been shown that they are especially useful when the number of unknowns is much greater than the amount of data (Tibshirani, Saunders, Rosset, Zhu and Knight (2005)), which is the case in the estimation of the PCD in tens of thousands of generators from only tens of data sensors.

Only a few approaches have attempted to use non-quadratic penalty terms, for example the Focal Underdetermined System Solver (FOCUSS) (Gorodnitsky and Rao (1997)) and the Controlled Support MEG (CSMEG) (Nagarajan, Portniaguine, Hwang, Johnson and Sekihara (2006)). Another approach added an autoregressive term to the LORETA functional to impose spatiotemporal constraints to the solution, giving rise to Dynamic LORETA, which is estimated via recursive penalized least squares regression (Yamashita, Galka, Ozaki, Biscay and Valdés-Sosa (2004)). Finally, some more sophisticated methods combine the penalized regression (or Tikhonov regularization) approach with other techniques using the Bayesian formalism, as is the case of the Bayesian Model Averaging solution presented in Trujillo-Barreto, Aubert-Vázquez and Valdés-Sosa (2004).

In this paper we use the penalized regression framework to introduce a general formulation of the IP of the EEG that contains several previous approaches as particular cases. This is called the multiple penalized least squares (MPLS) model and it allows one to address combinations of any number of penalty terms, quadratic or not (Valdés-Sosa, Sánchez-Bornot, Vega-Hernández, Melie-García, Lage-Castellanos and Canales-Rodríguez (2006)). The paper is structured as follows. In the next section we present the general MPLS model for the IP of the EEG, and we reinterpret the estimators given by using non-convex penalties as new types of inverse solutions. Some details on the algorithm used, and the quality measures for comparing different inverse solutions, are also presented.

The results of the comparative study are presented in the first half of the Section 3. The second half shows the application of the methodology to EEG recordings from a visual attention experiment. A final section is devoted to the discussion of results and conclusions of the study.

2. Multiple Penalized Least Squares Model

A general penalized linear regression can be written in the form (1.2), with a penalty term represented generically by $P(\mathbf{j})$:

$$\hat{\mathbf{j}} = \arg \min \left\{ \|\mathbf{v} - \mathbf{K}\mathbf{j}\|_2^2 + \lambda P(\mathbf{j}) \right\}.$$

The first term in the parentheses is a quadratic term that corresponds to the log-likelihood. The second term represents the constraint or penalization (known as prior information in the Bayesian framework), and λ is a weighting parameter that establishes the relative importance of the constraint. Different types of penalization can be imposed by introducing the corresponding additive terms in the functional leading to a general formulation of an EEG inverse solution as

$$\hat{\mathbf{j}} = \arg \min \left\{ \|\mathbf{v} - \mathbf{K}\mathbf{j}\|_2^2 + \sum \lambda_m P_m(\mathbf{j}) \right\}, \quad (2.1)$$

where $\sum \lambda_m P_m(\mathbf{j})$, with $m = 1 \dots M$, includes all prior information through the M penalty functions P_m . Each penalty term has a corresponding regularization parameter λ_m . Equation (2.1) sets forth the multiple penalized least squares (MPLS) model.

This formulation contains as particular cases several known inverse solutions, such as MN ($\hat{\mathbf{j}} = \arg \min \{ \|\mathbf{v} - \mathbf{K}\mathbf{j}\|_2^2 + \|\mathbf{I}\mathbf{j}\|_2^2 \}$, with \mathbf{I} the identity matrix) and LORETA ($\hat{\mathbf{j}} = \arg \min \{ \|\mathbf{v} - \mathbf{K}\mathbf{j}\|_2^2 + \|\mathbf{L}\mathbf{j}\|_2^2 \}$, with \mathbf{L} a discrete version of the 3D Laplacian operator, Table 2 of the supplemental material). All inverse solutions presented in Table 1 of the supplemental material, as well as FOCUSS, CSMEG and Dynamic LORETA can also be rewritten in the form of (2.1) and thus are particular cases of this formulation. In the latter case, unlike our approach, the temporal information of the solution is also taken into account which leads to a state-space model that is solved with a recursive penalized least squares regression. However, the spatiotemporal model may also be estimated by Kalman filtering which can be combined with non-convex penalty functions in order to decrease the computational burden.

The use of non-convex penalty functions defines several new types of inverse solutions. In this work we explore the performance of a subset of the best known in the linear regression field, together with the LORETA and MN solutions. The new solutions, according to penalty term, are as follows.

- **Least Absolute Shrinkage Selection Operator (LASSO)** (Tibshirani (1996)). The LASSO penalty is the l_1 -norm of the coefficients to estimate; thus,

the estimator takes the form $\hat{\mathbf{j}}_{LASSO} = \arg \min\{\|\mathbf{v} - \mathbf{K}\mathbf{j}\|_2^2 + \lambda\|\mathbf{j}\|_1\}$. This penalty forces the solution to be sparse, so as an inverse solution it should provide concentrated sources.

- **LASSO Fusion (LFusion)** (Land and Friedman (1996)). The LFusion is similar to LASSO but, in this case, the penalty function is the l_1 -norm of a linear operation on the coefficients. It can be written as $\hat{\mathbf{j}}_{LFusion} = \arg \min\{\|\mathbf{v} - \mathbf{K}\mathbf{j}\|_2^2 + \lambda\|\mathbf{D}\mathbf{j}\|_1\}$, where \mathbf{D} is the 3D gradient operator, given in Table 2 of the supplemental material online. This choice makes LFusion capable of dealing with group behavior by minimizing the first-order finite differences of coefficients, and providing piece-wise flat solutions. It can be seen that LFusion and LASSO are members of the family of methods using a penalty function of the form $\|\mathbf{H}\mathbf{j}\|_1$, where \mathbf{H} can be any positive definite matrix. Of particular interest is the case of higher order difference operators, due to ease of interpretation.

- **Smoothly Clipped Absolute Deviation (SCAD)** (Fan and Li (2001)). This method is defined by its penalty's derivative as $p'_{SCAD}(|j_i|) = \lambda\{\mathfrak{I}(|j_i| \leq \lambda) + ((a\lambda - |j_i|)_+ / (a - 1)\lambda)\mathfrak{I}(|j_i| > \lambda)\}$ for some $a > 2$, $i = 1, \dots, 3Ng$, where $(x)_+ = x$, (for $x \geq 0$), $(x)_+ = 0$, (for $x < 0$) and $\mathfrak{I}(\cdot)$ is the indicator function. This penalty function is designed to not excessively penalize large value coefficients and to make the solution continuous. Again, a general formulation is possible with the use of a linear operator $\mathbf{H}\mathbf{j}$ replacing \mathbf{j} in the expression above. Here we use the discrete 3D Laplacian operator for finding an inverse solution that will be called SCAD L.

- **LASSO Fused (LFused)** (Tibshirani, Saunders, Rosset, Zhu and Knight (2005)). This is a penalty derived from the combination of LASSO and LFusion. The solution is then given by $\hat{\mathbf{j}}_{LFused} = \arg \min\{\|\mathbf{v} - \mathbf{K}\mathbf{j}\|_2^2 + \lambda_1\|\mathbf{j}\|_1 + \lambda_2\|\mathbf{H}\mathbf{j}\|_1\}$. The idea here is to be able to recover sparse solutions in which there is group behavior, in addition to some isolated nonzero points. The use of different linear operators \mathbf{H} leads to the recovery of different properties for those points in the groups. Here we use the 3D Laplacian operator.

- **Ridge Fused (RFused)**. In the same flavor of the previous method, we propose a penalty that combines the penalties for MN and LORETA, which are two versions of Ridge. Analogously, we call it Ridge Fused and the estimator is $\hat{\mathbf{j}}_{RFused} = \arg \min\{\|\mathbf{v} - \mathbf{K}\mathbf{j}\|_2^2 + \lambda_1\|\mathbf{j}\|_2^2 + \lambda_2\|\mathbf{L}\mathbf{j}\|_2^2\}$. It is obvious that this penalty will not lead to sparse solutions but, depending on the weighting parameter, it can offer blurred solutions with intermediate properties between LORETA and MN.

- **Elastic Net (ENET)** (Zou and Hastie (2005)). This method is based on the combined use of a quadratic penalty and an l_1 -norm term. The original estimator is $\hat{\mathbf{j}}_{ENET} = \arg \min\{\|\mathbf{v} - \mathbf{K}\mathbf{j}\|_2^2 + \lambda_1\|\mathbf{j}\|_1 + \lambda_2\|\mathbf{j}\|_2^2\}$. However, we take the more general formulation $\hat{\mathbf{j}}_{ENET} = \arg \min\{\|\mathbf{v} - \mathbf{K}\mathbf{j}\|_2^2 + \lambda_1\|\mathbf{H}_1\mathbf{j}\|_1 + \lambda_2\|\mathbf{H}_2\mathbf{j}\|_2^2\}$, where \mathbf{H}_1 and \mathbf{H}_2 are full rank matrices. The version of ENET we test here

uses the discrete 3D Laplacian operator for both \mathbf{H}_1 and \mathbf{H}_2 , we refer to it as ENET L. This kind of combination is trying to achieve solutions in which there are patches of nonzero coefficients with smooth behavior, thus trying to get at the same time a mixture of smoothness and sparsity.

2.1. Implementation by a modified MM algorithm and selection of the regularization parameter

The MPLS model can be identified with the use of modified Newton-Raphson (NR) algorithms, such as Minorization-Maximization (MM) which extends the central idea of Expectation-Maximization algorithms to situations not necessarily involving ‘missing data’, nor even maximum likelihood estimation (Hunter and Li (2005) and Hunter and Lange (2004)). This algorithm inherits the virtues of the NR method, but cannot deal with the simultaneous use of several different penalties. To overcome this difficulty, our group recently introduced a generalized MM method for use in the estimation of massive autoregressive models of neuroimaging data (Valdés-Sosa, Sánchez-Bornot, Vega-Hernández, Melie-García, Lage-Castellanos and Canales-Rodríguez (2006)). We use it here for estimating the various inverse solutions.

An important issue in finding any inverse solution is the selection of the regularization parameter. In this paper, we use a grid of regularization parameters, and choose the value minimizing the generalized cross-validation function (GCV) (Golub, Heath and Wahba (1979)). It should be noted that, in the case of inverse solutions that use more than one penalty term, one must look for optimal values of all regularization parameters at the same time, requiring a multi-dimensional grid search. This is the case for Lfused, Rfused and ENET, for each of which we use a convenient reformulation of the problem for avoiding an exhaustive search that would increase computations prohibitively. The parameters involved are rewritten as $\lambda_1 = \lambda f_1$ and $\lambda_2 = \lambda f_2$. We then select only a few pairs of proportions f_1 and f_2 such that $f_1 + f_2 = 1$, and estimate an optimal value of λ by GCV. This allows the study of the dependence of the method on relative weights of quadratic and non-convex penalties, while keeping the same relative weight between the error fitting and total prior information.

2.2. Quality measures for evaluating inverse solutions

We use three measures (Pascual-Marqui (1999) and Trujillo-Barreto, Aubert-Vázquez and Valdés-Sosa (2004)) to evaluate the reconstruction of a simulated PCD by the methods in study. The first measures the ability to correctly localize the maximum value of the PCD. It is known as **Localization Error**, and defined as the Euclidean distance (in mm) between the maximum values of the estimated and real current densities: $Err = \|\mathbf{r}_{true} - \mathbf{r}\|$, where \mathbf{r}_{true} and \mathbf{r} denote the vector position of the maximum of real and estimated PCD, respectively.

The spatial dispersion of the solution can be measured by the **Blurring**. Here we compute the ratio between the full width at half maximum (FWHM) of the estimated and real current densities: $Blurr = FWHM/FWHM_{true}$ (Trujillo-Barreto, Aubert-Vázquez and Valdés-Sosa (2004)). The FWHM was defined in Fuchs, Wagner, Kohler and Wischman (1999) as the volume of voxels with strength above 50% of the maximum PCD (number of voxels times the volume of a voxel) divided by the total volume of the brain.

The third measure is the **Visibility**, defined as the ratio between the maximum values of estimated and simulated PCD: $Vis = \max(PCD)/\max(PCD_{true})$. Due to conservation of energy, this measure is related to Blurring, since more concentrated sources tend to have higher values and, similarly, the more distributed the sources, the lower the maximum value of the PCD. For a convenient presentation of the results, these measures were transformed to values between 0 and 1, being 1 only when the measure has the same value for the real and estimated PCD. The transformed measures are as follows: $EN = 1 - (Err/2R_b)$; $BN = \exp(2 - (Blurr + (1/Blurr)))$; $VN = \exp(2 - (Vis + (1/Vis)))$, where R_b is the radius of the brain (95 mm for the fitted sphere used in this work). Hereinafter we refer to these magnitudes as the normalized quality measures.

3. Validation of the Methodology

3.1. Simulation study

A grid of 3,862 points defined in the gray matter of the Brain Atlas of the Montreal Neurological Institute (Evans, Collins, Mills, Brown, Kelly and Peters (1993)) was used for constructing four different sets of current density distributions. Each set consisted of 5 simulated PCDs: a “central” PCD with maximum located in a particular anatomical structure, and the others derived from this one by moving the maxima in just one grid point. Maxima values of the “central” simulated PCDs were located in the cingulate region left (Cingulate), inferior temporal gyrus right (Temporal), occipital pole left (Occipital) and postcentral gyrus (Postcentral), as shown in Figure 3.1 of the supplemental material (online). All PCDs were simulated as a three-dimensional Gaussian source with the same amplitude and spatial dispersion. The Talairach coordinates for the twenty simulations are shown in Table 3 of the supplemental material (online). The Lead Field for this brain was computed as described in Riera and Fuentes (1998) for an array of 19 electrodes from the 10/20 system. The simulated voltages were obtained through equation (1.1), adding white noise in order to have a signal-to-noise ratio (SNR) of 30.

Eight different inverse solutions (MN, LORETA, RFused, LASSO, LFusion, LFused, SCAD L and ENET L) were computed for each simulated data set. Sagittal views in the coordinate of the maximum value of PCDs estimated by

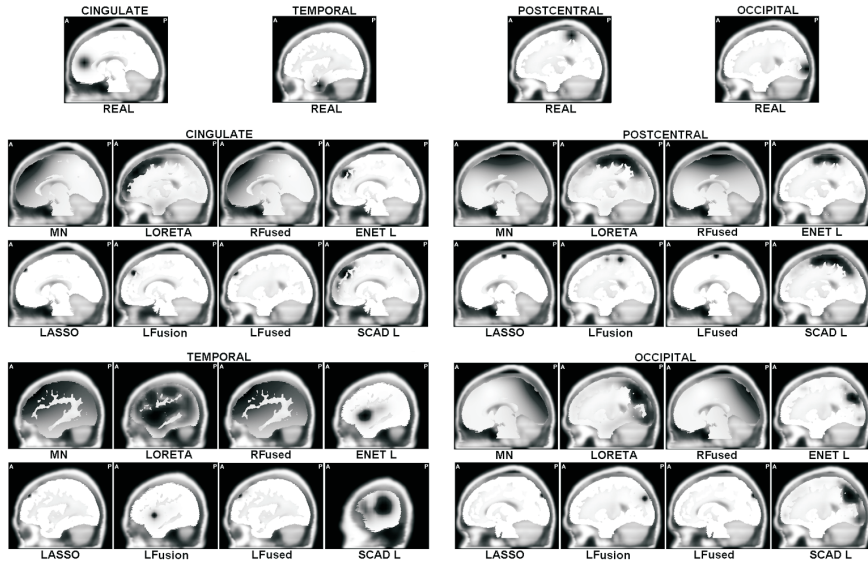


Figure 1. Top row: Sagittal views of the four central simulated PCD as three-dimensional Gaussians with maxima in different regions inside the brain. In all cases the amplitude and width of the Gaussians are fixed to 10 nA/mm^2 and 10 mm , respectively. Orthogonal views and coordinates of the maxima are shown in Figure 3.1 of the supplemental material (online). Middle and bottom rows: Sagittal views of eight different inverse solutions from the “central” simulated data in the anatomical locations cingulate, postcentral, temporal and occipital. Grayscale plotting uses white for zero current density and black for the maximum value of the PCD. These solutions can be viewed in color in Figure 3.2 of the supplemental material (online).

each method for every “central” simulated data set are presented in Figure 1. In all cases the optimal regularization parameter was found automatically by minimizing the GCV, and the proportions between weights for different penalties in LFused, RFused and ENET L were set to 1, i.e. $f_1 = f_2 = 0.5$.

Three-dimensional maps defined by the normalized quality measures computed for all inverse solutions found from the four “central” simulated data set are shown in Figure 2. In these plots the method with better general performance is the one with coordinates nearest to $[1, 1, 1]$. Also, in order to study the stability of the estimated solutions, we computed the mean and standard deviation of the normalized quality measures across the 5 inverse solutions common to a simulation set. These values, and the mean coefficient of variation, are shown in Table 1 of this manuscript and Table 4 of the supplemental material (online) respectively. The corresponding mean values of optimal λ 's and GCV's are shown also in Table 4 of the supplemental material (online).

Table 1. Mean \pm standard deviation of normalized Localization Error (EN), Blurring (BN) and Visibility (VN) of the five inverse solutions for each synthetic data set. Best and second best numbers are bold faced.

	OCCIPITAL			POSTCENTRAL		
	EN	BN	VN	EN	BN	VN
MN	0.51 ± 0.36	0.54 ± 0.12	0.70×10^{-3} $\pm 1.51 \times 10^{-3}$	0.59 ± 0.09	0.59 ± 0.19	3.43×10^{-3} $\pm 4.57 \times 10^{-3}$
LORETA	0.51 ± 0.30	0.41 ± 0.08	2.60×10^{-5} $\pm 5.79 \times 10^{-5}$	0.60 ± 0.15	0.48 ± 0.08	4.04×10^{-3} $\pm 6.35 \times 10^{-3}$
RFused	0.51 ± 0.36	0.53 ± 0.12	0.69×10^{-3} $\pm 1.48 \times 10^{-3}$	0.59 ± 0.09	0.59 ± 0.19	3.37×10^{-3} $\pm 4.49 \times 10^{-3}$
LASSO	0.40 ± 0.31	0.71 ± 0.18	1.12×10^{-2} $\pm 0.99 \times 10^{-2}$	0.63 ± 0.17	0.58 ± 0.21	4.39×10^{-3} $\pm 9.21 \times 10^{-3}$
LFusion	0.41 ± 0.31	0.58 ± 0.22	0.41 ± 0.26	0.58 ± 0.14	0.54 ± 0.22	0.23 ± 0.15
LFused	0.47 ± 0.37	0.67 ± 0.17	0.45 ± 0.34	0.69 ± 0.18	0.60 ± 0.19	0.34 ± 0.26
SCAD L	0.56 ± 0.37	0.72 ± 0.15	5.55×10^{-2} $\pm 4.90 \times 10^{-2}$	0.62 ± 0.09	0.65 ± 0.18	4.97×10^{-2} $\pm 3.18 \times 10^{-2}$
ENET L	0.47 ± 0.37	0.96 ± 0.07	0.45 ± 0.21	0.70 ± 0.18	0.94 ± 0.08	0.62 ± 0.12
	CINGULATE			TEMPORAL		
	EN	BN	VN	EN	BN	VN
	0.61 ± 0.25	0.50 ± 0.14	1.68×10^{-3} $\pm 2.30 \times 10^{-3}$	0.45 ± 0.06	0.52 ± 0.14	1.43×10^{-5} $\pm 1.90 \times 10^{-5}$
LORETA	0.73 ± 0.20	0.30 ± 0.07	0.89×10^{-3} $\pm 1.57 \times 10^{-3}$	0.54 ± 0.15	0.36 ± 0.10	2.04×10^{-5} $\pm 4.55 \times 10^{-5}$
RFused	0.61 ± 0.25	0.50 ± 0.14	1.65×10^{-3} $\pm 2.26 \times 10^{-3}$	0.45 ± 0.06	0.52 ± 0.14	1.40×10^{-5} $\pm 1.92 \times 10^{-5}$
LASSO	0.72 ± 0.15	0.76 ± 0.20	1.27×10^{-2} $\pm 1.77 \times 10^{-2}$	0.42 ± 0.05	0.75 ± 0.13	0.21 ± 0.26
LFusion	0.84 ± 0.02	0.83 ± 0.15	0.43 ± 0.26	0.50 ± 0.16	0.55 ± 0.24	0.63 ± 0.30
LFused	0.83 ± 0.02	0.84 ± 0.16	0.45 ± 0.33	0.46 ± 0.07	0.71 ± 0.12	0.68 ± 0.17
SCAD L	0.74 ± 0.21	0.54 ± 0.13	0.06 ± 0.11	0.53 ± 0.09	0.72 ± 0.19	0.11 ± 0.19
ENET L	0.84 ± 0.01	0.90 ± 0.09	0.55 ± 0.20	0.54 ± 0.14	0.99 ± 0.01	0.30 ± 0.21

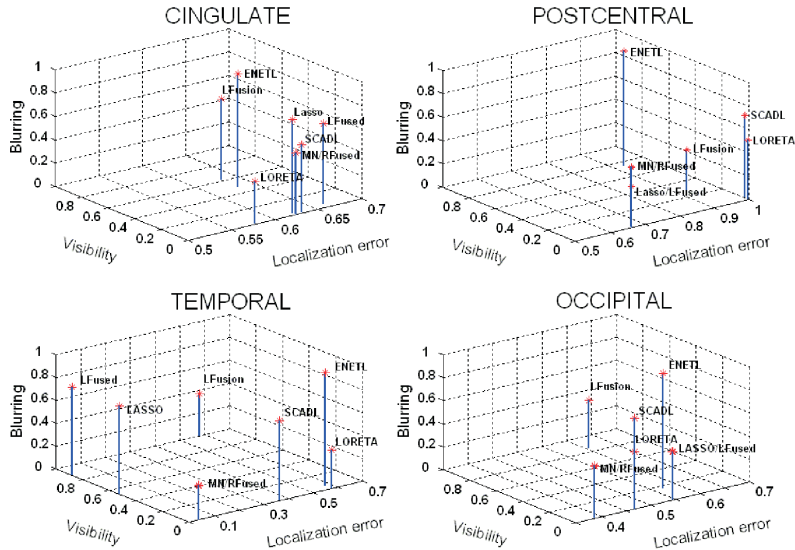


Figure 2. 3D maps of inverse solutions on the space of normalized quality measures (values between 0 and 1). Axes are chosen to get the best view of the position of each inverse solution in the graph. Better reconstruction performances correspond to higher values of all normalized quality measures.

The MN, LORETA and RFused always offered more blurred solutions than the simulated PCD, and correspondingly less Visibility. On the other hand, LASSO, LFusion and LFused gave very concentrated solutions; they do not allow for correct estimation of the blurring of the real PCD, and usually give maximum values of the PCD higher than simulated ones. Therefore, in all these cases, BN and VN have values far from 1. The SCAD L and ENET L methods offer solutions with middle values for blurring, nearer to the real one while the visibility and localization errors are acceptable. In a general view, ENET L seems to show the best performance among these eight methods.

3.2. Source localization of evoked potentials

We analyzed the data provided by the EEGLAB Toolbox (Delorme and Makeig (2004)), which is freely available at <http://scn.ucsd.edu/eeglab/eeglabtut.html>. This data set corresponds to the study of the attention modulation of the early visual components. Other details of the experiment and processing of the data can be found in Section 4 of the supplemental material (online). The topography was obtained at the latency corresponding to the so-called N1 peak (281 ms after the presentation of the stimulus) for source localization through three inverse solutions: LORETA, LFusion and ENET L. The optimal regularization parameters were selected by minimization of the GCV criterion. In the case of

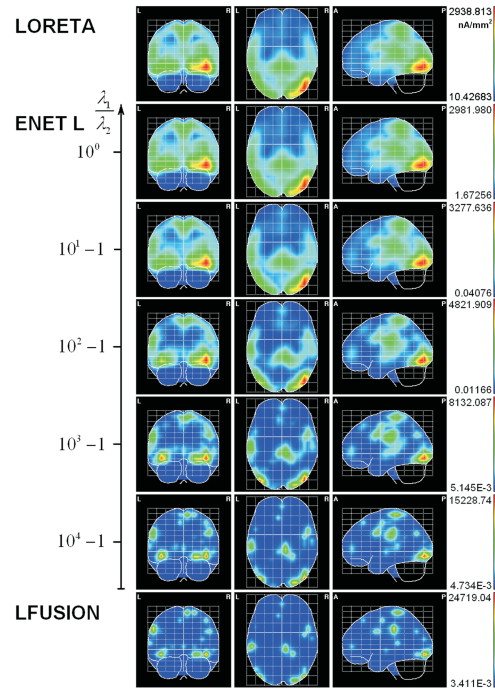


Figure 3. Estimated PCD of the N1 peak by LORETA, LFusion and ENET L. In the case of ENET L, five solutions are shown for different proportions of weights corresponding to non-quadratic and quadratic penalties. The color scale indicates maximum and minimum values for each solution. Note that concentrated sources have higher maximum values. Corresponding values of optimal regularization parameters and GCV are shown in Table 5 of the supplemental material (online).

ENET, we explored different proportions of weights for quadratic and non-quadratic terms in order to control the amount of smoothness and sparsity of the solution.

Figure 3 shows the maximum projection in orthogonal planes of the estimated PCD by the three methods. It can be seen that as the proportion between weights in ENET L ($\lambda_1/\lambda_2 = f_1/f_2$) decreases, the estimated solution goes from a very sparse to a very smooth one showing in essence the same sources. In other words, tuning the proportion λ_1/λ_2 in ENET L allows intermediate solutions to LORETA and LFusion, controlling the blurring of the PCD. Optimal values for the regularization parameters and corresponding GCV can be found in Table 5 of the supplemental material (online).

In spite of the extended use of inverse solutions for localizing neural sources of evoked components, the noisy nature of the data and the ill-posed character of the IP have raised the requirement of a statistical post-processing for assessing

the significant activations of neural sources (Bosch-Bayard, Valdés-Sosa, Virués-Alba, Aubert-Vázquez, John, Harmony, Riera-Díaz and Trujillo-Barreto (2001) and Pascual-Marqui, Esslen, Kochi and Lehmann (2002)). It has been also argued that this can help to eliminate ghost sources commonly offered by linear inverse solutions (Grave de Peralta and González (1998)). In this work we computed a Hotelling's T^2 statistic in each voxel from the inverse solutions for 80 trials of the N1 peak to find significant activations (Carbonell, Galá, Valdés-Sosa, Worsley, Biscay, Díaz-Comas, Bobes and Parra (2004)).

Figure 4 shows the Hotelling's T^2 images for the same methods presented in Figure 3. The images have been thresholded with a Bonferroni correction for the comparison of 3,862 voxels with a p-value of 0.05. Significant activations were localized mainly in the occipital areas in all cases, although other sources are

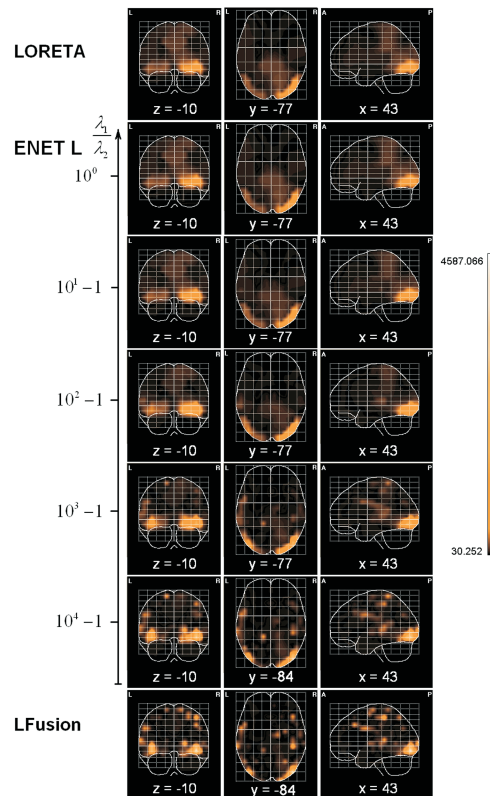


Figure 4. Images of the Hotelling's T^2 statistic from inverse solutions of 80 trials of the N1 peak. The methods LORETA, LFusion and ENET L are shown in the same way as in Figure 3. The color scale shows the global maximum value of the T^2 among all statistical images and the lower threshold, which corresponds to a p-value of 0.05 corrected for multiplicity (Bonferroni). Talairach coordinates of the voxel with maximum T^2 statistic in each case are shown below the corresponding images.

also present in the cases of such very sparse solutions as LFusion and ENET L, with the highest ratio of weights. The Talairach coordinates of the voxel with maximum T^2 value are also shown.

4. Discussion and Conclusions

The simulations support the following general view: LASSO and LFusion can be interpreted as the concentrated versions of MN and LORETA, respectively, since they presented similar localization of the maximum PCD. Conservation of energy implies that concentrated sources have higher values, thus generally improving the visibility of the solutions. These solutions have better spatial resolution and are good choices in those cases in which the existence of small activated areas are known a priori. However, this effect also enhances ghost sources (already present in MN and LORETA as part of the main activation, see Figure 1 and Figure 3.3 of the supplemental material (online)) that appear more clearly and with higher values. This is also the case for SCAD L (at least in the study presented here), which produced less blurred solutions than LORETA with similar localization error. On the other hand, methods based on combination of penalties such as RFused and LFused offer more adaptive solutions, but depend strongly on the regularization parameters. They always showed solutions very similar to LASSO and MN, respectively, with maxima in voxels at the surface of the brain, thus biasing deep sources. Furthermore, ENET L was able to recover solutions with almost the same blurring as the simulated PCD.

In the comparative study among these inverse solutions (for the “central” simulated data) in terms of normalized quality measures, ENET L always showed the best Blurring and LFusion the best Visibility, while both have similar Localization Error (see Figure 2). In Table 1 the two highest means in each column are highlighted. ENET L was the best or the second-best method in 10 of the 12 cases. Since this penalty consists of a mixture of the LORETA penalty and LFusion penalty, it preserves the good localization properties of LORETA, diminishing the blurring of the solution and, correspondingly, increasing the visibility. This improvement of the combined penalty with respect to each penalty separately (LORETA and LFusion) has been previously described for ENET by Zou and Hastie (2005). Moreover, in terms of the stability of solutions, we found that ENET L showed the lowest average coefficient of variation (across the three quality measures) in three simulation sets, being the second lowest in the remaining set. LFusion, LFused and SCAD L also showed low values of coefficient of variation. In contrast, the GCV procedure was not so stable. Optimal values of regularization parameters varied over a wide range for different solutions, as shown in Table 4 of the supplemental material (online). This is a well-known problem of the regularization approach that requires further development.

The combined properties of ENET L solutions were more apparent in the analysis of sources of the N1 peak appearing in the average evoked potential of a visual attention experiment (Figure 4). It is evident that tuning the proportion of penalties in ENET L produces solutions ranging from pure LORETA to pure LFusion. The maximum activation was found in the lateral occipitotemporal gyrus, which is consistent with previous reports in the literature (Makeig, Westerfield, Jung, Enghoff, Townsend, Courchesne and Sejnowskii (2002) and Di Russo, Martínez, Sereno, Pitzalis and Hillyard (2001)). However, what seems to be a unique source widely spread from occipital to parietal and temporal areas, as shown by LORETA, becomes an image of several small concentrated sources in all those areas as shown by LFusion. Therefore, in the latter case the appearance of ghost sources (sources with no physiological meaning) is made clearer by the requirement of sparsity of the solution. In this sense, ENET L allows intermediate solutions in terms of the blurring and appearance of ghost sources. Particularly, in our example, we could say that the solution corresponding to a ratio of $10^2 - 1$ ($f_1 = 0.99$, $f_2 = 0.01$) between weights of l_1 and l_2 -norm terms, is the one with the more concentrated main source without showing ghost sources. This selection is made here by visual inspection, since these data are used for illustration purposes, although some criteria should be sought for selecting which is the most appropriate proportion of weights according to the data at hand.

In summary, in this work we have introduced a general formulation of the EEG inverse problem, in the form of a multiple penalized least squares model. With MPLS the use of non-convex penalties leads to new inverse solutions which are sparse, i.e., show concentrated sources, improving the spatial resolution and interpretability of separate generators. Furthermore, the combination of several penalties produces more adaptive solutions. In particular, we found that the ENET inverse solution showed the best general performance among all tested methods and was able to recover adaptively concentrated and blurred sources by tuning the proportion of corresponding weights parameters. This property makes ENET L a promising method for the search of generators of a wide variety of neurocognitive processes.

However, it should be said that a full exploration of the validity of the new methods as inverse solutions was not addressed here. We hope that the preliminary studies carried out motivate a more thorough study on the use of non-convex penalties and combination of them as inverse solutions. Several drawbacks still affect the methodology presented. For example, although the inverse solutions based on combination of penalties showed better performance than individual solutions separately, it should be noted that they are more dependent on the appropriate selection of regularization parameters. On the other hand, the modified MM algorithm used here is still not optimal in terms of efficiency, and it could take several minutes to estimate a solution based on mixtures of penalties.

This, together with the need for 50 to 100 runs with different regularization parameters in order to evaluate the GCV function, makes the search for a more efficient and fast algorithm a goal for future research. Finally, other penalties which have been proposed from a Bayesian point of view for achieving sparsity, can be introduced in the proposed model, for example the double exponential (Vidakovic (1998)) and Normal-Jeffrey (Kiiveri (2003)) prior.

Acknowledgement

The authors gratefully acknowledge Dr. Lídice Galán for her useful comments and the revision of the manuscript.

References

- Bosch-Bayard, J., Valdés-Sosak, P., Virués-Alba, E., Aubert-Vázquez, E., John, E. R., Harmony, T., Riera-Díaz, J. and Trujillo-Barreto, N. (2001). 3D statistical parametric mapping of variable resolution electromagnetic tomography (VARETA). *Clin. Electroencephal.* **32**, 47-66.
- Carbonell, F., Galán, L., Valdés-Sosa, P., Worsley, K., Biscay, R. L., Díaz-Comas, L., Bobes, M. A. and Parra, M. (2004). Random field-union intersection tests for EEG/MEG imaging. *NeuroImage.* **22**, 268-276.
- Craven, P. and Wahba, G. (1979). Smoothing noisy data with spline functions: estimating the correct degree of smoothing by the method of generalized cross-validation. *Numer. Math.* **31**, 377-403.
- Delorme, A. and Makeig, S. (2004). EEGLAB: an open source toolbox for analysis of single-trial EEG dynamics including independent component analysis. *J. Neurosci. Meth.* **134**, 9-21.
- Di Russo, F., Martínez, A., Sereno, I. M., Pitzalis, S. and Hillyard, S. A. (2001). Cortical sources of the early components of the visual evoked potential. *Hum. Brain Mapp.* **15**, 95-111.
- Evans, A. C., Collins, D. L., Mills, S. R., Brown, E. D., Kelly, R. L. and Peters, T. M. (1993). 3D statistical neuroanatomical models from 305 MRI volumes. *Proc. IEEE-Nuclear Science Symposium and Medical Imaging Conference.* **95**, 1813-1817. M.T.P Press, London.
- Fan, J. Q. and Li, R. Z. (2001). Variable selection via nonconcave penalized likelihood and its oracle properties. *J. Amer. Statist. Assoc.* **96**, 1348-1360.
- Fuchs, M., Wagner, M., Wischman, H. A. and Dossel, O. (1995). *Cortical current imaging by morphologically constrained reconstructions*. In Biomagnetism: Fundamental Research and Clinical Applications (Edited by C. Baumgartner, et al.), 320-325, Elsevier: Science IOS Press.
- Fuchs, M., Wagner, M., Kohler, T. and Wischman, H. A. (1999). Linear and nonlinear current density reconstructions. *J. Clin. Neurophysiol.* **16**, 267-295.
- Grave de Peralta, R. and González, S. L. (1998). Basic limitations of linear inverse solutions: a case study. *IEEE Eng. Med. Biol.* **4**, 2143-2146.
- Gorodnitsky, I. F. and Rao, B. D. (1997). Sparse signal reconstruction from limited data using FOCUSS: are-weighted minimum norm algorithm. *IEEE T Signal Proces.* **45**, 600-616.
- Golub, G., Heath, M. and Wahba, G. (1979). Generalized cross-validation as a method for choosing a good ridge parameter. *Technometrics* **21**, 215-223.

- Hadamard, J. (1923). Lecture on the Cauchy problem in linear partial differential equations. Yale University Press, New Haven, CT.
- Hämäläinen, M. S. and Ilmoniemi, R. J. (1994). Interpreting magnetic fields of the brain: minimum norm estimates. *Med. Biol. Eng. Comput.* **32**, 35-42.
- Hansen, P. C. (1992). Analysis of discrete ill-posed problems by means of the L-Curve. *SIAM Rev.* **34**, 561-580.
- Hoerl, A. E. and Kennard, R. W. (2000). Ridge Regression: biased estimation for nonorthogonal problems. *Technometrics* **42**, 80-86.
- Hunter, D. R. and Lange, K. (2004). A tutorial on MM algorithms. *Amer. Statist.* **58**, 30-37.
- Hunter, D. R. and Li, R. (2005). Variable selection using MM algorithms. *Ann. Statist.* **33**, 1617-1642.
- Kiiveri, H. (2003). *A Bayesian approach to variable selection when the number of variables is very large*. In Science and Statistics: Festschrift for Terry Speed (Edited by D. R. Goldstein). Institute of Mathematical Statistics Lecture Note-Monograph Series. **40**, 127-143.
- Land, S. and Friedman, J. (1996). Variable fusion: a new method of adaptive signal regression. *Technical Report. Department of Statistics, Stanford University, Stanford*.
- Makeig, S., Westerfield, M., Jung, T.-P., Enghoff, S., Townsend, J., Courchesne, E. and Sejnowskii, T. J. (2002). Dynamic brain sources of visual evoked responses. *Science*. **295**, 690-694.
- Nagarajan, S. S., Portnaguine, O., Hwang, D., Johnson, C. and Sekihara, K. (2006). Controlled support MEG imaging. *NeuroImage* **33**. 878-885.
- Pascual-Marqui, R. D., Michel, C. M. and Lehmann, D. (1994). Low resolution electromagnetic tomography: a new method for localizing electrical activity in the brain. *Int. J. Psychophysiol.* **18**, 49-65.
- Pascual-Marqui, R. D. (1999). Review of methods for solving the EEG inverse problem. *Inter J. Bioelectromagnetism.* **1**, 75-86.
- Pascual-Marqui, R. D., Esslen, M., Kochi, K. and Lehmann, D. (2002). Functional imaging with low-resolution brain electromagnetic tomography (LORETA): A review. *Method Find. Exp. Clin.* **24**, 91-95.
- Riera, J. J. and Fuentes, M. E. (1998). Electric lead field for a piecewise homogeneous volume conductor model of the head. *IEEE Trans. Biomed. Eng.* **45**, 746-753.
- Scherg, M. and von Cramon, D. (1986). Evoked dipole source potentials of the human auditory cortex. *Electroen. Clin. Neuro.* **65**, 344-360.
- Scholz, B. and Schwierz, G. (1994). Probability-based current dipole localization from biomagnetic fields. *IEEE T. Bio-Med. Eng.* **41**, 735-742.
- Tibshirani, R. (1996). Regression shrinkage and selection via the LASSO. *J. Roy. Statist. Soc. Ser. B* **58**, 267-288.
- Tibshirani, R., Saunders, M., Rosset, S., Zhu, J. and Knight, K. (2005). Sparsity and smoothness via the fused lasso. *J. Roy. Statist. Soc. Ser. B* **67**, 91-108.
- Trujillo-Barreto, N., Aubert-Vázquez, E. and Valdés-Sosa, P. A. (2004). Bayesian model averaging in EEG/MEG imaging. *NeuroImage*. **21**, 1300-1319.
- Valdés-Sosa, P., Marti, F., Garcia, F. and Casanova, R. (2000). Variable resolution electric-magnetic tomography. *Biomag 96. Proc. of the Tenth International Conference on Biomagnetism*, II, 373-376, Springer-Verlag, New York.

- Valdés-Sosa, P. A., Sánchez-Bornot, J. M., Vega-Hernández, M., Melie-García, L., Lage-Castellanos, A. and Canales-Rodríguez, E. (2006). *Granger Causality on Spatial Manifolds: Applications to Neuroimaging*. Handbook of Time Series Analysis: Recent Theoretical Developments and Applications, chapter 18. ISBN: 3-527-40623-9.
- Vidakovic, B. (1998). *Wavelet-Based Nonparametric Bayes Methods* .. In Practical Nonparametric and Semiparametric Bayesian Statistics (Edited by D. Dey, P. Muller and D. Sinha), 133-156, Springer-Verlag, New York.
- Yamashita, O., Galka, A., Ozaki, T., Biscay, R. and Valdés-Sosa, P. A. (2004). Recursive penalized least squares solution for the dynamical inverse problem of EEG generation. *Hum. Brain Mapp.* **21**, 221–235.
- Zou, H. and Hastie, T. (2005). Regularization and variable selection via the elastic net. *J. Roy. Statist. Soc. Ser. B* **67**, 301.

Neurostatistics Department, Cuban Neuroscience Center, Havana, Cub.

E-mail: mayrim@cneuro.edu.cu

Neurostatistics Department, Cuban Neuroscience Center, Havana, Cub.

E-mail: eduardo@cneuro.edu.cu

Neurostatistics Department, Cuban Neuroscience Center, Havana, Cub.

E-mail: bornot@cneuro.edu.cu

Neurostatistics Department, Cuban Neuroscience Center, Havana, Cub.

E-mail: agustin@cneuro.edu.cu

Neurostatistics Department, Cuban Neuroscience Center, Havana, Cub.

E-mail: peter@cneuro.edu.cu

(Received April 2007; accepted December 2007)